

Effects of the local structure on a cracked periodically distributed composite

M. Patrício¹, R. Mattheij¹ and G. de With²

Abstract: In this paper the effect of the local structure of a highly heterogeneous composite material on the parameters that characterise crack propagation is analysed. The evaluation of stress intensity factors is discussed. A hybrid approach based on domain decomposition and homogenisation methods is employed to obtain accurate solutions with reduced computational complexity.

Keywords: Composite material, fracture, stress intensity factor, homogenisation, domain decomposition.

1 Introduction

Engineering structures are designed to withstand the loads they are expected to be subject to while in service. Large stress concentrations are avoided and a reasonable margin of security is taken to ensure that values close to the maximum admissible stress are never attained. However, material imperfections which arise at the time of production or usage of the material are unavoidable, and hence must be taken into account. Indeed, even microscopic flaws may cause structures which are otherwise safe to fail, as they grow over time.

In the past, when a component of some structure exhibited a crack, it was either repaired or simply retired from service. Such precautions are nowadays in many cases deemed unnecessary, not possible to enforce, or may prove too costly. In this setting fracture mechanics plays a central role, as it provides useful tools which allow for an analysis of materials which exhibit cracks, Broek (1986); Cherepanov (1979); Freund (1990); Owen and Fawkes (1983). The goal is to predict whether and in which manner failure might occur.

In this paper we shall focus on the brittle fracture of composite materials with periodically distributed linear elastic components. The increasing usage of composites

¹ Department of Mathematics and Computer Science, Technische Universiteit Eindhoven

² Department of Chemical Engineering and Chemistry, Technische Universiteit Eindhoven

for high performance applications has justified much interest in recent years, cf. for example Aymerich and Serra (2006); Guz, J.Rushchitsky, and A.Guz (2008); Fitzgerald, Goldbeck-Wood, Kung, Petersen, Subramanian, and J.Wescott (2008, 2004); Masuda and Noguchi (2006). We are particularly interested in ascertaining the value of the stress intensity factors (SIFs) of a loaded cracked plate - see for example Aliabadi and López (1996); H. Tada and Irwin (2000). The SIFs are relevant material parameters for elastic materials as it can be assumed that crack propagation will occur when they reach certain values. In general, a fracture criteria such as this allow the modelling of crack growth, see for example Sageresan and Drathi (2008); Wang and Wang (2008); Gato and Shie (2008); A. Dimitrov and Schnack (2006).

The elastic behaviour of the materials we look into can be modelled as a boundary value problem for which the underlying differential equation has highly oscillating ε -periodic coefficients. Finding the solution of these problems, which is a prior requirement to the computation of the SIFs, is complicated from a numerical point of view. Indeed, for small values of ε , the usage of finite elements is no longer feasible. Taking an element size smaller than the typical periodicity is required in order to obtain accurate results, cf. Hou, Wu, and Cai (1999), but that would be computationally too expensive.

To address this issue one may resort to the theory of homogenisation, Cioranescu and Donato (1999); Pavliotis and Stuart (2007). With this, one finds a macroscopic constitutive equation for a homogenised medium which captures the average behaviour of the composite. The advantage of this procedure is that the boundary value problem obtained with the new constitutive equation is no longer ε -dependent. However, the role of the heterogeneities is disregarded. It is then not possible to obtain good estimates for the SIFs, as these depend greatly on the local structure.

In this paper we consider heterogeneous materials with pre-existing cracks. Each crack tip is laying fully inside one of the components of the composite material. Our goal is to approximate the stress and displacement fields of the elastic plate accurately, so that good approximations for the SIFs can be found.

We start by formulating the elasticity problem for a composite material in Section 2. There the classical notions of fracture mechanics that will be employed are introduced. In Section 3 the stress field around a crack tip, for which the SIFs play a fundamental role, is characterised. We show how to compute these material parameters. In particular the stress correlation method, the displacement correlation method and the J-integral are applied. Next, in Section 4, we investigate the effect of the local structure of a periodically distributed composite material on the value of the stress intensity factors, for several example microstructures. An algorithm

that combines homogenisation and domain decomposition techniques is presented, cf. Patrício, Mattheij, and de With (2008b). This allows for an accurate and computationally cheap way to determine the SIFs, in particular for small values of ε , for one or more cracks. Finally, in Section 5, a plate of a heterogeneous material with a central crack is considered. For different crack lengths, the SIFs are computed using the aforementioned algorithm.

2 The mechanisms of linear elastic fracture

In this section we first introduce the equations that describe the behaviour of a composite plate Ω with constituents periodically distributed. Let us assume that Ω is covered by a mosaic of cells of the form $\varepsilon Y =]0, \varepsilon l_1[\times]0, \varepsilon l_2[$ over which the material is distributed as in the reference cell $Y =]0, l_1[\times]0, l_2[$, cf. Patrício, Mattheij, and de With (2008a).

In the absence of body forces the well-known linear elasticity problem for the composite material is stated as follows, cf. Cioranescu and Donato (1999)

$$\begin{cases} -\nabla \cdot (\mathbf{A}^\varepsilon(\mathbf{x})\varepsilon(\mathbf{u}^\varepsilon)) = \mathbf{0}, & \mathbf{x} \in \Omega, \\ \mathbf{u}^\varepsilon = \mathbf{0}, & \text{on } \Gamma_D, \\ \boldsymbol{\sigma}(\mathbf{u}^\varepsilon) \cdot \mathbf{n} = \mathbf{g}_N, & \text{on } \Gamma_N, \end{cases} \quad (1)$$

where \mathbf{g}_N is a given vector function. As for $\varepsilon = (\varepsilon_{ij})_{i,j=1,2}$ and $\boldsymbol{\sigma} = (\sigma_{ij})_{i,j=1,2}$, they are the strain and stress tensors defined respectively by

$$\varepsilon(\mathbf{w}) = (\nabla \mathbf{w} + (\nabla \mathbf{w})^T), \quad \boldsymbol{\sigma}(\mathbf{w}) = \mathbf{A}^\varepsilon \varepsilon(\mathbf{w}), \quad (2)$$

for any vector function \mathbf{w} taking values over Ω . The tensor \mathbf{A}^ε characterising the behaviour of the material can be obtained by extending the components of a fourth-order tensor $\tilde{\mathbf{A}} = \tilde{\mathbf{A}}(\mathbf{y}) = (\tilde{a}_{ijkl})_{1 \leq i,j,k,h \leq 2}$, defined over the reference cell Y , periodically to \mathbb{R}^2 . We denote $\mathbf{A}^\varepsilon = \mathbf{A}^\varepsilon(\mathbf{x}) = (a_{ijkl}^\varepsilon)_{1 \leq i,j,k,h \leq N}$ such that for $\mathbf{x} = (x_1, x_2) \in \mathbb{R}^2$, one has $a_{ijkl}^\varepsilon(\mathbf{x}) := \tilde{a}_{ijkl}(\mathbf{y}) = \tilde{a}_{ijkl}(\mathbf{x}/\varepsilon)$, where $\mathbf{y} := \mathbf{x}/\varepsilon$, for $\mathbf{y} = (y_1, y_2) \in \mathbb{R}^2$.

Now consider a plate Ω , with elastic behaviour described by (1), exhibiting a crack. The mechanisms of crack propagation lay outside the scope of the theory of elasticity. It is useful to adopt Irwin's classical classification Irwin (1958a) corresponding to the three situations represented in Figure 1. It distinguishes the different ways a cracked plate may be loaded.

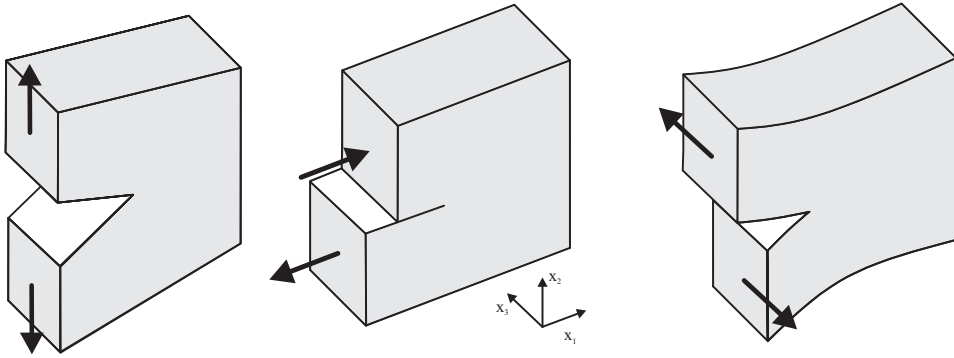


Figure 1 - a) Mode I.

b) Mode II.

c) Mode III.

Accordingly we consider three distinct modes: mode I, mode II and mode III.

For each of these modes crack extension may only take place in the direction of the x_1 -axis, the original orientation of the crack. More generally, we typically find a mixed mode situation, where there is a superposition of the modes and the crack may propagate in any direction. For such a problem the principle of stress superposition states that the individual contributions to a given stress component are additive, so that if σ_{ij}^I , σ_{ij}^{II} and σ_{ij}^{III} are the stress components associated to the modes I, II and III respectively, then the stress component σ_{ij} of a plate in a mixed mode situation is given by

$$\sigma_{ij} = \sigma_{ij}^I + \sigma_{ij}^{II} + \sigma_{ij}^{III}, \text{ for } i, j = 1, 2. \quad (3)$$

Within the scope of the theory of linear elasticity, a crack introduces a discontinuity in the elastic body such that the stresses tend to infinity as one approaches the crack tip. Using the semi-inverse method as in Westergaard (1939), Irwin Irwin (1957, 1958b) related the singular behaviour of the stress components to the distance to the crack tip r . In particular, when we consider a Cartesian coordinate system centred at the crack tip, in the mode I and in polar coordinates we have

$$\sigma_{ij} \simeq \frac{K_I}{\sqrt{2\pi r}} f_{ij}^I(\theta), \quad (4)$$

where the angular variation function f_{ij}^I , which will be introduced later, depends only on θ . The parameter K_I , the stress intensity factor, plays a fundamental role

in fracture mechanics, as it characterises the stress field, reflecting the geometry of the structure and the loading it is subject to. This approximation for the stresses is assumed to be valid in the vicinity of the crack tip for linearly elastic materials. Actually, the materials yield or deform inelastically very near the crack tip and so there is a region of validity of the approximation, cf. Zehnder (2007).

Henceforth we will consider the problem of elastic brittle fracture of a cracked plate in a plane stress situation, which means that mode III situations (pure or mixed) will be disregarded. Due to the presence of the crack, besides the equations of elasticity, an extra equation to serve as fracture criteria is also required, see for example, Broek (1986); Cherepanov (1979). Many different criteria are available in the literature. In what follows, we will adopt a classical criterium.

For a stationary semi-infinite line crack, loaded in a mode *I* situation, we assume that crack growth will occur when

$$K_I = K_{I_c} \quad (5)$$

holds. Here K_{I_c} , which behaves as a threshold value for K_I , is called the *critical stress intensity factor* or *mode I fracture toughness*. It may be determined experimentally for each material. In Table 1 we include examples of experimental data for the fracture toughness of some materials, as taken from Ashby and Jones (1996).

Table 1: Examples of fracture toughness.

Material	K_{I_c} ($MN/m^{3/2}$)
Mild steel	140
Titanium alloys	55 – 120
High carbon steel	30
Nickel, copper	> 100
Nickel, copper	> 100
Concrete (steel reinforced)	10 – 15
Concrete (unreinforced)	0.2
Glasses, rocks	1
Ceramics (Alumina, SiC)	3 – 5
Nylon	3
Polyester	0.5

We now focus our attention on the more general situation when the loading is a combination of modes *I* and *II*. Unlike the mode *I* loading situation, where the

direction of the crack growth is trivially determined, criteria on whether the crack will propagate but also on which direction it may do so must be decided upon. This will be based on the circumferential tensile stress $\sigma_{\theta\theta}$ which, up to an order of \sqrt{r} , reads

$$\sigma_{\theta\theta}(r, \theta) = \frac{K_{\theta\theta}(\theta)}{\sqrt{2\pi r}}, \quad (6)$$

where

$$K_{\theta\theta}(\theta) = K_I \cos^3\left(\frac{1}{2}\theta\right) - 3K_{II} \sin\left(\frac{1}{2}\theta\right) \cos^2\left(\frac{1}{2}\theta\right) \quad (7)$$

is the circumferential stress intensity factor, cf. Broek (1986); Cherepanov (1979). We assume that crack growth will occur when

$$\max_{\theta} K_{\theta\theta}(\theta) = K_{Ic}, \quad (8)$$

which can be seen as a generalisation of (5). The direction of propagation is given by the angle $\theta = \theta_p$ which maximizes $K_{\theta\theta}(\theta)$,

$$\theta_p = 2 \arctan \left(\frac{K_I - \sqrt{K_I^2 + 8K_{II}^2}}{4K_{II}} \right). \quad (9)$$

Note that using (9), (8) can be rewritten as

$$\frac{4\sqrt{2}K_{II}^3(K_I + 3\sqrt{K_I^2 + 8K_{II}^2})}{(K_I^2 + 12K_{II}^2 - K_I\sqrt{K_I^2 + 8K_{II}^2})^{\frac{3}{2}}} = K_{Ic}. \quad (10)$$

3 Determination of the SIF

The SIFs are fundamental parameters in the prediction of crack propagation. It is therefore important to be able to compute them accurately. We now look at several ways to do so.

3.1 Local and global approaches

In order to describe the local approach to determining the SIFs, we start by examining the role that they have in the distribution of stresses and displacements in the region around the tip of a crack. For that, consider a static crack in a plate which is in a plane stress situation. Assume that the crack is positioned along the negative x_1 -axis as in Figure 2 and that its surfaces are stress free.

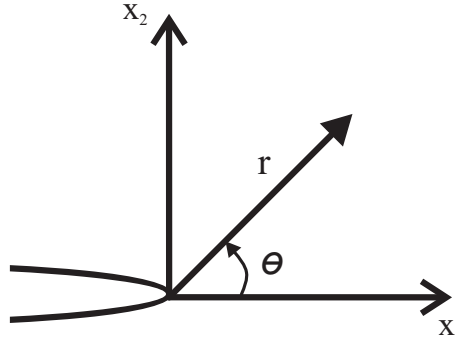


Figure 2: Crack tip coordinates.

Then the stress field in the vicinity of the crack tip is given, up to an order of \sqrt{r} , by

$$\sigma_{ij}(r, \theta) = \frac{K_I}{\sqrt{2\pi r}} f_{ij}^I(\theta) + \frac{K_{II}}{\sqrt{2\pi r}} f_{ij}^{II}(\theta), \quad (11)$$

see for example Broek (1986); Cherepanov (1979); Freund (1990); Irwin (1958a). Here, $i, j = 1, 2$. As for K_I and K_{II} , they are defined by

$$K_I := \lim_{r \rightarrow 0} K_I^*(r), \quad \text{where } K_I^*(r) = \sqrt{2\pi r} \sigma_{22}(r, 0), \quad (12)$$

$$K_{II} := \lim_{r \rightarrow 0} K_{II}^*(r), \quad \text{where } K_{II}^*(r) = \sqrt{2\pi r} \sigma_{12}(r, 0). \quad (13)$$

Finally, in (11), the angular variation functions for mode I are given by

$$f_{11}^I(\theta) = \cos\left(\frac{1}{2}\theta\right) \left(1 - \sin\left(\frac{1}{2}\theta\right) \sin\left(\frac{3}{2}\theta\right)\right), \quad (14)$$

$$f_{22}^I(\theta) = \cos\left(\frac{1}{2}\theta\right) \left(1 + \sin\left(\frac{1}{2}\theta\right) \sin\left(\frac{3}{2}\theta\right)\right), \quad (15)$$

$$f_{12}^I(\theta) = f_{21}^I(\theta) = \cos\left(\frac{1}{2}\theta\right) \sin\left(\frac{1}{2}\theta\right) \cos\left(\frac{3}{2}\theta\right), \quad (16)$$

while the equivalent functions for mode II are

$$f_{11}^{II}(\theta) = -\sin\left(\frac{1}{2}\theta\right) \left(2 + \cos\left(\frac{1}{2}\theta\right) \cos\left(\frac{3}{2}\theta\right)\right), \quad (17)$$

$$f_{22}^{II}(\theta) = \cos\left(\frac{1}{2}\theta\right) \sin\left(\frac{1}{2}\theta\right) \cos\left(\frac{3}{2}\theta\right), \quad (18)$$

$$f_{12}^{II}(\theta) = f_{21}^{II}(\theta) = \cos\left(\frac{1}{2}\theta\right) \left(1 - \sin\left(\frac{1}{2}\theta\right) \sin\left(\frac{3}{2}\theta\right)\right). \quad (19)$$

It is also possible to obtain equations for the corresponding displacement field near the crack tip, cf. Cherepanov (1979); Irwin (1958a); Owen and Fawkes (1983).

The formulas we have presented allow us to characterise the stress field in the vicinity of a crack tip. In turn, if the stress field is known, this allows for the determination of the SIFs using (12) and (13). This technique is called the stress correlation method. It is applied as follows: to calculate K_I , one simply finds the function $K_I^*(r)$ for values of the stress computed ahead of the crack tip and extrapolates the value of the function back to $r = 0$. In a similar way, $K_{II}^*(r)$ can also be determined. This method is quite simple, but its accuracy depends on the mesh refinement and also on how it deals with the crack singularity.

In turn, the displacement correlation method makes use of the equations for the displacement field near the crack tip. From these it can be shown that

$$K_I = \lim_{r \rightarrow 0} K_I^{**}(r), \text{ where } K_I^{**}(r) = \frac{E}{4} u_2(r, \pi) \sqrt{\frac{2\pi}{r}}, \quad (20)$$

$$K_{II} = \lim_{r \rightarrow 0} K_{II}^{**}(r), \text{ where } K_{II}^{**}(r) = \frac{E}{4} u_1(r, \pi) \sqrt{\frac{2\pi}{r}}, \quad (21)$$

where E is the Young's modulus of the elastic material where the crack tip lays, cf. Zehnder (2007).

One alternative to the above local approach is obtained by using the path-independent *J-integral* Rice (1968). This is defined as a line integral along a counterclockwise contour C which surrounds the crack tip, see Figure 3. Its components are given in terms of the strain energy density $W_e = \sum_{i,j=1,2} \sigma_{ij} \epsilon_{ij}$ and the stresses by

$$J_k = \oint_C (W_e n_k - \sum_{i,j=1,2} \sigma_{ij} n_j \frac{\partial u_i}{\partial x_k}) dS, \quad (22)$$

for $k = 1, 2$ and where $\mathbf{n} = (n_1, n_2)$ is the outward-pointing normal vector defined over C , cf. Hegen (1997); van Vroonhoven (1996); Zehnder (2007). The vector $\mathbf{J} = (J_k)_{k=1,2}$ can be regarded as the energy flux per unit length into the crack tip. It is called path-independent because it does not depend on the choice of the curve C .

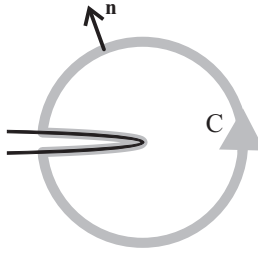


Figure 3: Integration path (gray) around the crack tip.

We note that in a mode I situation, once the J-integral has been computed, the SIF can also be obtained by

$$J = \frac{K_I^2}{E}, \quad (23)$$

cf. Hegen (1997); van Vroonhoven (1996); Zehnder (2007). The main advantage of the J-integral method is that it is in general very accurate without requiring the usage of very fine meshes. The reason for that is that capturing the crack tip singular stress field is no longer necessary. It suffices to be able to find a good approximation for the stress and strain fields over the curve C . It is in that sense a global approach.

3.2 Numerical approach

There are classical examples of cracked geometries for which the mode I SIFs have been computed or approximated explicitly and are available in handbooks, cf. H. Tada and Irwin (2000). Consider for example a square plate, of side length $2b$, with a central crack of length $2a$, see Figure 4. Let the plate be loaded from its upper and lower edges by a uniform tensile stress σ .

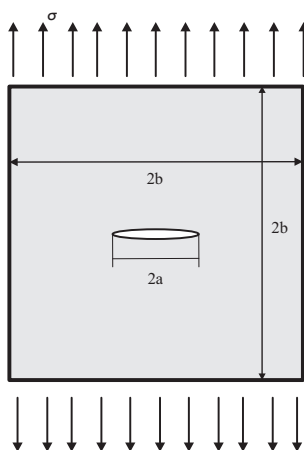


Figure 4: Finite plate with a centre through crack under tension.

An expression for the SIFs can be given by

$$K_I = \sigma\sqrt{\pi a}(1 + 0.043\rho + 0.491\rho^2 + 7.125\rho^3 - 28.403\rho^4 + 59.583\rho^5 - 65.278\rho^6 + 29.762\rho^7), \quad (24)$$

cf. Aliabadi Aliabadi and López (1996). From this formula we compute reference solutions for the stress intensity factors for several values of $\rho = a/b$. The values of K_I/K_0 , where $K_0 := \sigma\sqrt{\pi a}$, are displayed in the second line of Table 2. Note that K_I/K_0 does not depend on the loading applied to the plate, but only on the geometrical ratio ρ . In what follows we discuss several methods to compute the SIFs numerically, namely the stress correlation method, the displacement correlation method and the J-integral method, cf. for example Zehnder (2007).

We start by finding an approximation for the SIFs by applying the displacement correlation method. As a first step we need to solve the elasticity problem. In order

to do that we use finite elements. A mesh with quadratic triangular elements with maximum width of the element side $h = 0.01$ is generated. Now, for each value of ρ , we approximate the function K_I^{**} linearly within an interval contained in $[0, a]$. The choice of the interval is not arbitrary: since the limit for $r \rightarrow 0$ is sought, we want to consider the function in a domain where the values of r are small. On the other hand, the crack tip singularity affects the accuracy of the results near $r = 0$. This means that the values of K_I^{**} when r is too small must be disregarded.

To illustrate this procedure, we take $\rho = 0.4$. Without loss of generality, let $b = 1$. The values of K_I^{**}/K_0 can be plotted versus the values of r , see the full line in Figure 5.

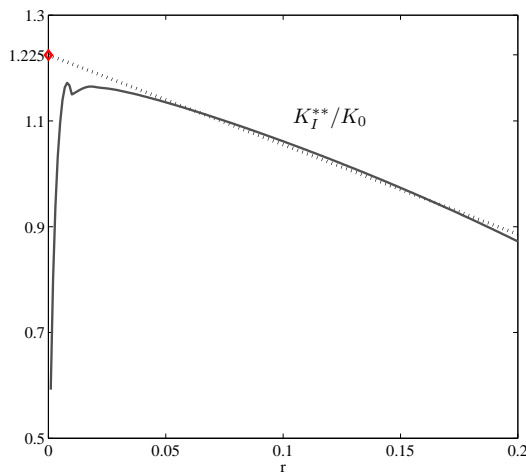


Figure 5: Extrapolation using the displacement correlation method, $\rho = 0.4$.

We use a linear interpolator - represented by a dashed line- to fit the function in the interval $[0.03, 0.2]$. The data over the interval $[0, 0.03]$ are neglected due to the crack tip singularity. To proceed, we extrapolate the value of the interpolator back to $r = 0$, in order to obtain the desired approximation. The SIFs obtained using this method are displayed in the third line of Table 2 for the different values of ρ contained in the first line of the table.

The stress correlation method goes about in a similar way. The respective results are shown in the fourth line of Table 2. They are not so accurate as the previous results. This was to be expected, because we are using the stresses to approximate the SIFs, whereas the primary result of the finite element analysis is the displacement field.

Table 2: Stress intensity factors.

SIF/ $K_0 \setminus \rho$	0.1	0.2	0.4	0.6
K_I	1.014	1.055	1.216	1.481
$K_I(\mathbf{u})$	1.004	1.058	1.225	1.525
$K_I(\boldsymbol{\sigma})$	1.226	1.145	1.211	1.802
$K_I(J)$	1.004	1.051	1.212	1.477

It should be pointed out that the choice of the interval where the linear interpolator is to be applied does affect the results, as it is not completely objective and requires intuition. The inherent subjectivity of the choice of an interval is no longer a problem for the method employing the J-integral, as this fracture parameter is path-independent. In this sense this is a much more reliable method than the previous two as it allows for quite accurate approximations of the SIFs. The results obtained using this method can be seen in the last line of Table 2. They are given by (23) after averaging a number of J-integrals, each computed over a small circle centred at the crack tip.

4 SIFs in composite materials

In what follows we investigate how the local structure of a highly heterogeneous plate influences the SIFs of a pre-existent static crack. A hybrid approach to compute these fracture parameters is included.

4.1 Effects of the local structure

Consider a cracked plate $\Omega = \Omega_p - \Omega_C$, where $\Omega_p = [-0.5, 0.5] \times [-0.5, 0.5]$ and Ω_C is the crack line $[-0.5, -0.3] \times \{0\}$ of length $a = 0.2$, see Figure 6.

The plate is made of a composite elastic material, its elastic behaviour being modelled by (1). We assume that the plate is pulled at its upper and lower edges. The remaining boundaries, including the crack edges, are stress-free, so that the following boundary conditions hold

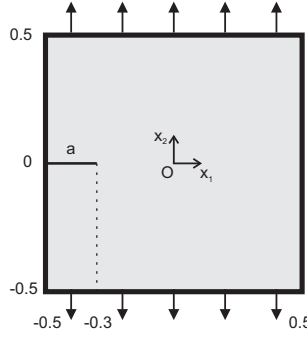


Figure 6: Cracked plate.

$$g_N(\mathbf{x}) = \begin{cases} (0, 1), & x_2 = 0.5, \\ (0, -1), & x_2 = -0.5, \\ (0, 0), & \text{otherwise.} \end{cases} \quad (25)$$

Let the plate be composed of a layered material with isotropic constituents with components of the elasticity tensor \tilde{A} reading

$$\tilde{a}_{2222}(\mathbf{y}) = \tilde{a}_{1111}(\mathbf{y}) = \frac{E(\mathbf{y})}{1 - \nu^2(\mathbf{y})}; \quad \tilde{a}_{2211}(\mathbf{y}) = \frac{E(\mathbf{y})\nu(\mathbf{y})}{1 - \nu^2(\mathbf{y})}; \quad (26)$$

$$\tilde{a}_{2121}(\mathbf{y}) = \frac{E(\mathbf{y})}{2(1 + \nu(\mathbf{y}))}; \quad \tilde{a}_{2111}(\mathbf{y}) = \tilde{a}_{2221}(\mathbf{y}) = 0, \quad (27)$$

where E is the Young's modulus, ν is the Poisson's ratio and $\mathbf{y} = (y_1, y_2)$. We assume that the reference cell for this material, given by $Y = [0, 1] \times [0, 1]$, can be decomposed into two subdomains $Y_1 = [0, 0.5] \times [0, 1]$, $Y_2 = [0.5, 1] \times [0, 1]$ composed respectively by materials A and B, see Figure 7. Moreover, for $i = 1, 2$, Y_i is occupied by a linear elastic material with Young's modulus $E_i = E_i(y_1)$ and Poisson's ratio $\nu_i = \nu_i(y_1)$. In short, we have

$$E(\mathbf{y}) = E_1\chi_1(y_1) + E_2\chi_2(y_1), \quad (28)$$

$$\nu(\mathbf{y}) = \nu_1\chi_1(y_1) + \nu_2\chi_2(y_1), \quad (29)$$

where χ_1 and χ_2 are the characteristic functions of the sets Y_1 and Y_2 . These are defined by

$$\chi_i(\mathbf{y}) = \begin{cases} 1, & \text{for } \mathbf{y} \in Y_i, \\ 0, & \text{for } \mathbf{y} \in Y - Y_i, \end{cases} \quad (30)$$

and can be extended periodically.

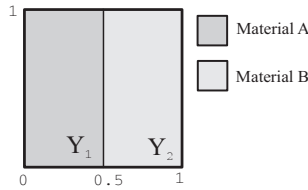


Figure 7: The reference cell Y , composed of two different materials.

Finally let

$$v_1 = 0.3, \quad v_2 = 0.1, \quad E_1 = 10, \quad E_2 = 1, \quad \varepsilon = 0.02. \quad (31)$$

The problem we have described up to now has been set up so that the material layers are disposed orthogonally to the crack line, see Figure 8 e). We actually want to think of other material orientations as well, in order to illustrate the effect of the local structure on the SIFs. We consider the five situations depicted in Figure 8, which represent zoom-ins of the vicinity of the crack tip. The figures labeled a) to e) correspond to the different material orientations characterised by the angles $\beta = 0^\circ, 30^\circ, 45^\circ, 60^\circ$ and 90° that the layer boundaries form with the horizontal axis. Furthermore we assume that the crack tip lays inside material A.

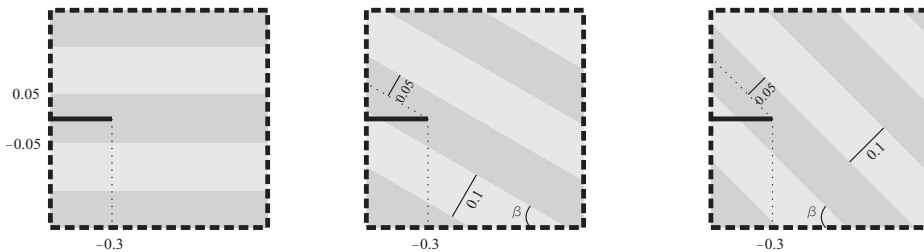
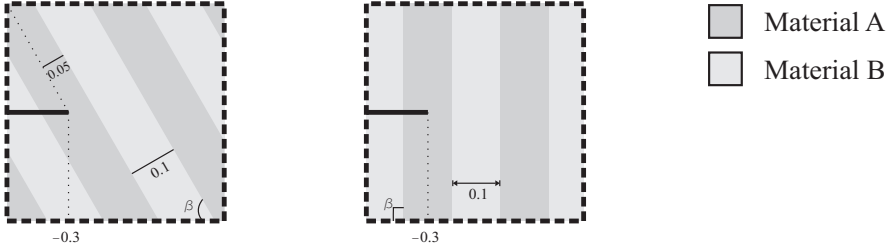


Figure 8 - a) $\beta = 0^\circ$

b) $\beta = 30^\circ$.

c) $\beta = 45^\circ$.



d) $\beta = 60^\circ$.

e) $\beta = 90^\circ$.

For each of these configurations, our goal is to compute the SIFs K_I and K_{II} as well as the propagation angle θ_p . Before we can compute the SIFs, we have to solve the elasticity problems (1) with (25)-(31) for the various values of β . For that we employ the finite element method. A fine mesh with quadratic triangular elements in the vicinity of the crack tip and quadratic rectangular elements everywhere else is generated. This allows for the computation of the displacement and stress fields for the different material orientations. The SIFs K_I and K_{II} are then determined using the J-integral method and their values are displayed in Table 3. As for the propagation angle θ_p also included in the table, it is zero when $\beta = 0^\circ$ or $\beta = 90^\circ$. In the other cases, it is computed using (9).

Table 3: SIF and propagation angle. The material surrounding the crack tip is characterised by E_1 and ν_1 .

β	K_I	K_{II}	θ_p
0°	2.20	0	0°
30°	2.13	$-2.23E - 2$	1.2°
45°	2.10	$-5.22E - 2$	2.8°
60°	2.11	$-8.20E - 2$	4.4°
90°	2.13	0	0°

Next, we interchange the roles of materials A and B. We assume they are now characterised by E_2 and ν_2 and by E_1 and ν_1 respectively. We solve the previous problem with this new assumption. The values we find are shown in Table 4.

Table 4: SIF and propagation angle. The material surrounding the crack tip is characterised by E_2 and ν_2 .

β	K_I	K_{II}	θ_P
0°	$8.16E - 1$	0	0°
30°	$7.75E - 1$	$7.18E - 2$	-10.4°
45°	$7.10E - 1$	$1.07E - 1$	-16.4°
60°	$6.24E - 1$	$1.21E - 1$	-20.5°
90°	$5.39E - 1$	0	0°

By comparing the results in the two tables, it can be seen that the local structure can influence the value of the SIFs quite dramatically. For this example of a layered material, this may not be so much the case when the material orientation changes. Indeed, if we take for instance the values of K_I along the second column of Table 3 or of Table 4 they do not vary much. However, there is quite a difference when the crack tip is laying on different materials. This is particularly relevant for composites or other materials which are very heterogeneous.

We note that we dealt with a heterogeneous periodic plate where the period ε of the heterogeneities was rather large. For this accurate numerical approximations of the solutions of the elasticity problems and consequently of the SIFs could be obtained by the finite element method and taken as reference solutions. When ε is much smaller, the typical mesh width h must satisfy $h \ll \varepsilon$ to yield reasonable results and so prohibitively thin meshes have to be employed. Alternatively, we may adopt a macroscopic approach and replace the heterogeneous medium by a fictitious equivalent homogeneous material. In particular, instead of the layered material with vertically disposed layers for which (28) and (29) hold, one may consider the orthotropic material characterised by the elasticity tensor \bar{A} with components

$$\bar{a}_{1111} = \frac{E_x}{1 - \nu_{xy}\nu_{yx}}, \quad \bar{a}_{2211} = \frac{E_x\nu_{yx}}{1 - \nu_{xy}\nu_{yx}}, \quad (32)$$

$$\bar{a}_{2222} = \frac{E_y}{1 - \nu_{xy}\nu_{yx}}, \quad \bar{a}_{2121} = G_{xy}, \quad (33)$$

$$\bar{a}_{2111} = \bar{a}_{2221} = 0, \quad (34)$$

where $\nu_{xy}E_y = \nu_{yx}E_x$, cf. Patrício, Mattheij, and de With (2008a). Homogenisation can also be applied for the remaining material orientations other than for $\beta = 90^\circ$, by rotating the axes of orthotropy.

The advantage of the homogenisation procedure lays in the very significant simplification of the underlying elasticity equations, as the ε -dependent coefficients are replaced by constants. However this comes at the price of losing the effects of locality. Indeed, homogenisation intends to provide the average behaviour of a material in some sense, not its local behaviour, so it is not as accurate. Moreover, we note that if we are interested in computing the SIFs and propagation angles for the homogenised material it should be taken into account that the homogenised material is orthotropic. In particular, the maximum circumferential tensile stress criterion (8) should be reformulated, cf. Nobile and Carloni (2005).

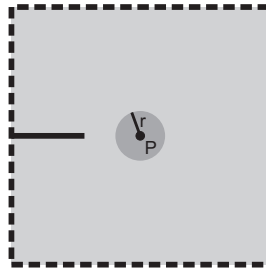


Figure 9: Inclusion near the crack tip.

Besides the material orientation, the behaviour of the SIFs is also affected by the presence of defects, as we will illustrate in the following example. Consider again the cracked plate represented in Figure 6, and let it now be composed of a linear elastic isotropic homogeneous material with $E = 1$ and $\nu = 0.1$. We assume that it is subject to the boundary conditions (25), so that a mode I situation arises. Using the J-integral method to compute the SIF for this configuration, we find that $K_I = 1.18$.

Now consider the same plate but containing one linear elastic circular inclusion of radius 0.05, centred at the point P and characterised by $E_2 = 10$ and $\nu_2 = 0.3$, cf. Figure 9. We take various coordinates for P as listed in Table 5, so that the SIF can be measured when the inclusion is closer or further from the crack tip, located at $(-0.3, 0)$.

When the inclusion is at a larger distance d from the crack tip, the SIF is about the same as the one computed for the plate without any inclusion. Conversely, this fracture parameter is affected by a closer proximity of the inclusion, see Table 5.

Table 5: SIF affected by the proximity of an inclusion.

P	d	K_I
$(-0.2, 0)$	0.05	1.11
$(-0.1, 0)$	0.15	1.16
$(-0.2, 0.2)$	0.17	1.14
$(-0.1, 0.2)$	0.23	1.15
$(0, 0)$	0.25	1.17
$(0.2, 0)$	0.45	1.18

This example illustrates the sensitivity of the stress intensity factors to the local characteristics of the surroundings of the crack tip. If one looks for accurate approximations for the SIFs, the local structure in the vicinity of the crack tip may not be disregarded. As we move away from this region, the heterogeneities have much less influence on the crack behaviour.

4.2 Hybrid approach

The heterogeneities of composite materials should be taken into account in order for accurate enough approximations for the SIFs to be obtained. However, doing so explicitly with the use of finite elements is in most cases too demanding in terms of the computational complexity.

To deal with this one would like to have the best of both worlds and design a method that is both accurate - especially in the vicinity of the crack tip - and computationally feasible. This is the goal of the hybrid approach presented in Patrício, Mattheij, and de With (2008b). This is a flexible method which allows the region around the crack tip to be treated separately. It is also easily adaptable for when there is more than one crack present.

The idea of this hybrid approach is to employ both homogenisation and domain decomposition methods. Then, instead of approaching (1) directly, we split the domain Ω in Ω_1 and $\Omega_2 = \Omega - \Omega_1$, where Ω_1 is a small region that surrounds the crack tip. On Ω_2 we want to use the ε -periodicity of the composite material to approximate the solution with homogenisation techniques. As for Ω_1 , it is a critical region where accuracy is fundamental, and it is important to solve the heterogeneities fully.

The hybrid approach for this problem can be expressed in the form of an algorithm. Following Patrício, Mattheij, and de With (2008b), we will introduce a sequence of problems defined on two overlapping subdomains $\hat{\Omega}_1$ and Ω_2 , where $\Omega_1 \subset \hat{\Omega}_1 \subset \Omega$. Let $\Gamma_1 = \partial\Omega_1 \cap \partial\Omega_2$ and $\Gamma_2 = \partial\hat{\Omega}_1 \cap \partial\Omega_2$, as illustrated in Figure 10.

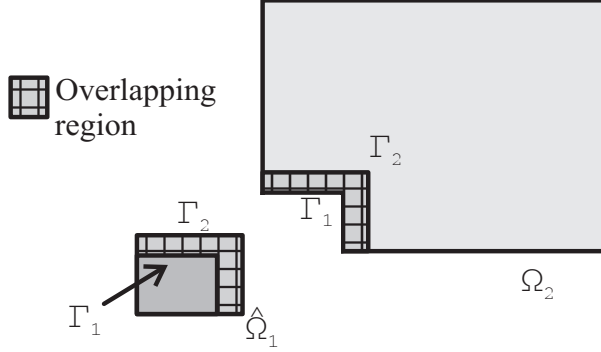


Figure 10: The overlapping subdomains $\hat{\Omega}_1$ and Ω_2 .

The domain $\hat{\Omega}_1$ must be chosen so that the overlapping region $\hat{\Omega}_1 - \Omega_1$ suits our needs. One should take into account that choosing this region to be large implies that the iterative scheme converges in less steps. However, there is a trade off, as more effort must be put into solving the problem on $\hat{\Omega}_1$.

The algorithm expressing the hybrid approach for elasticity, allowing us to obtain sequences of approximations $\{\hat{\mathbf{u}}_1^{(k)}\}_k$ and $\{\hat{\mathbf{u}}_2^{(k)}\}_k$ for $\mathbf{u}^\varepsilon|_{\hat{\Omega}_1}$ and $\mathbf{u}^\varepsilon|_{\Omega_2}$, respectively, is as follows. Let $\hat{\lambda}^{(0)}$ be the initial guess for $\mathbf{u}|_{\Gamma_2}$, $\mathbf{Tol} = (Tol_1, Tol_2)$ the tolerance for the stopping condition and $k = 0$.

1 - Solve

$$\left\{ \begin{array}{ll} -\nabla \cdot (\mathbf{A}^\varepsilon \boldsymbol{\varepsilon}(\hat{\mathbf{u}}_1^{(k+1)})) = \mathbf{0}, & \mathbf{x} \in \hat{\Omega}_1, \\ \hat{\mathbf{u}}_1^{(k+1)} = \mathbf{0}, & \mathbf{x} \in \Gamma_D \cap \partial\hat{\Omega}_1, \\ \boldsymbol{\sigma}(\hat{\mathbf{u}}_1^{(k+1)}) \cdot \mathbf{n} = g_N, & \mathbf{x} \in \Gamma_N \cap \partial\hat{\Omega}_1, \\ \hat{\mathbf{u}}_1^{(k+1)} = \hat{\lambda}^{(k)}, & \mathbf{x} \in \Gamma_2, \end{array} \right. \quad (35)$$

and

$$\begin{cases} -\nabla \cdot (\bar{\mathbf{A}}\boldsymbol{\varepsilon}(\bar{\mathbf{w}}^{(k+1)})) = \mathbf{0}, & \mathbf{x} \in \Omega_2, \\ \bar{\mathbf{w}}^{(k+1)} = \mathbf{0}, & \mathbf{x} \in \Gamma_D \cap \partial\Omega_2, \\ \boldsymbol{\sigma}(\bar{\mathbf{w}}^{(k+1)}) \cdot \mathbf{n} = g_N, & \mathbf{x} \in \Gamma_N \cap \partial\Omega_2, \\ \bar{\mathbf{w}}^{(k+1)} = \hat{\mathbf{u}}_1^{(k+1)}, & \mathbf{x} \in \Gamma_1. \end{cases} \quad (36)$$

2 - Set

$$\mathbf{w}_1(\mathbf{x}) = \frac{1}{2} \sum_{i,j=1,2} \left(\frac{\partial \bar{w}_i}{\partial x_j} + \frac{\partial \bar{w}_j}{\partial x_i} \right) \chi^{ij} \left(\frac{\mathbf{x}}{\boldsymbol{\varepsilon}} \right). \quad (37)$$

3 - Solve

$$\begin{cases} -\nabla \cdot (\bar{\mathbf{A}}\boldsymbol{\varepsilon}(\mathbf{C}^{(k+1)})) = \mathbf{0}, & \mathbf{x} \in \Omega_2, \\ \mathbf{C}^{(k+1)} = -\boldsymbol{\varepsilon}\mathbf{w}_1, & \mathbf{x} \in \Gamma_D \cap \partial\Omega_2, \\ \boldsymbol{\sigma}(\mathbf{C}^{(k+1)}) \cdot \mathbf{n} = \mathbf{0}, & \mathbf{x} \in \Gamma_N \cap \partial\Omega_2. \end{cases} \quad (38)$$

$$4 - \text{Set } \hat{\mathbf{u}}_2^{(k+1)} := \bar{\mathbf{w}}^{(k+1)} + \boldsymbol{\varepsilon}\mathbf{w}_1^{(k+1)} + \mathbf{C}^{(k+1)}.$$

5 - Update $\hat{\boldsymbol{\lambda}}^{(k)}$ and increment k

$$\hat{\boldsymbol{\lambda}}^{(k+1)} = \hat{\mathbf{u}}_2^{(k+1)}|_{\Gamma_2}, \quad (39)$$

$$k \rightarrow k + 1. \quad (40)$$

6 - Return to step 1 until

$$\|(\hat{\mathbf{u}}_1^{(k)}|_{\Gamma_2} - \hat{\mathbf{u}}_2^{(k)}|_{\Gamma_2})_i\|_{\infty} < Tol_i, \text{ for } i = 1, 2. \quad (41)$$

Here, $(\hat{\mathbf{u}}_1^{(k)}|_{\Gamma_2} - \hat{\mathbf{u}}_2^{(k)}|_{\Gamma_2})_i$ represents the i^{th} component of the vector function $(\hat{\mathbf{u}}_1^{(k)}|_{\Gamma_2} - \hat{\mathbf{u}}_2^{(k)}|_{\Gamma_2})$. We may take Tol_1 and Tol_2 as the estimated maximum homogenisation errors for the horizontal and vertical components of the displacement, respectively. Finally, χ and \mathbf{C} denote the solution of the cell problem and boundary corrector associated to (1), respectively. For more details see Patrício, Mattheij, and de With (2008b).

We note that this algorithm may be significantly simplified if the accuracy requirements are not too demanding. The iteration steps 2 to 4, where correctors are employed to improve the accuracy of the overall procedure, may be replaced by simply having $\widehat{\mathbf{u}}_2^{(k+1)} := \overline{w}^{(k+1)}$. In any case the error originating from this procedure will depend on the accuracy of the homogenised solution, which improves for smaller values of ε .

Finally, we note that a possible choice for an initial approximation $\widehat{\lambda}^{(0)}$ is given by $\widehat{\lambda}^{(0)} := \overline{u}|_{\Gamma_2}$, where

$$\begin{cases} -\nabla \cdot (\overline{A}\varepsilon(\overline{u})) = \mathbf{0}, & \mathbf{x} \in \Omega, \\ \overline{u} = \mathbf{0}, & \mathbf{x} \in \Gamma_D, \\ \boldsymbol{\sigma}(\overline{u}) \cdot \mathbf{n} = \mathbf{g}_N, & \mathbf{x} \in \Gamma_N. \end{cases} \quad (42)$$

This particular initial guess provides a cheap approximation for the solution of (1) by disregarding the heterogeneities.

With this hybrid procedure the computational complexity of the original problem is significantly reduced, as the heterogeneities are only resolved where it is relevant to do so.

5 Numerical example

To approximate the stress intensity factors for a given crack, using the computational methods mentioned in section 3, it is necessary to first solve the elasticity problem. For very heterogeneous materials, the complexity of this task is tackled by the hybrid approach.

To illustrate the relevant features of this technique, we consider a cracked elastic plate $\Omega = \Omega_P - \Omega_C$, where $\Omega_P = [-1, 1] \times [-1, 1]$ and Ω_C is the closed crack line $[-a, a] \times \{0\}$.

We assume that the plate is composed of a layered material with vertically disposed isotropic components such that (1) and (28)-(29) hold. Besides this, we take

$$v_1 = v_2 = 0.3, \quad E_1 = 3, \quad E_2 = 1, \quad \varepsilon = 2.5E - 2. \quad (43)$$

As for the boundary conditions, let the plate be pulled along its upper and lower edges while it remains free of stress along the other boundaries so that

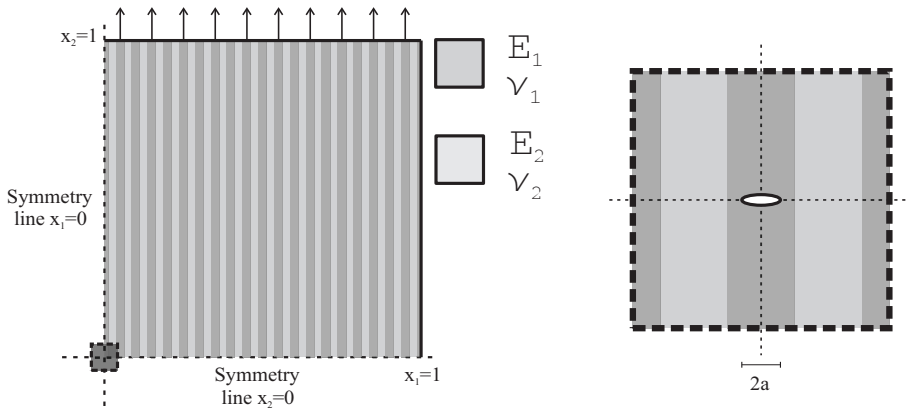


Figure 11: Cracked plate (left) and zoom-in around crack region (right).

$$g_N(\mathbf{x}) = \begin{cases} (0, 1), & x_2 = 1, \\ (0, -1), & x_2 = -1. \\ (0, 0), & \text{otherwise.} \end{cases} \quad (44)$$

Due to the underlying symmetry of the problem, it suffices to consider the domain $[0, 1] \times [0, 1] - ([0, a] \times \{0\})$ represented on Figure 11.

Consider the values for a , half of the crack length, included in the first line of Table 6. For each of these values, a reference solution is found for the elasticity problem employing finite elements, with very fine meshes. Using the J-integral method, the mode I stress intensity factor K_I is computed. It is included in the second line of the table.

Table 6: Mode I stress intensity factor.

	$2.5E-3$	$5.0E-3$	$7.5E-3$	$1.0E-2$
K_I	$1.33E-1$	$1.93E-1$	$2.46E-1$	$3.24E-1$
K_I^{ha}	$1.31E-1$	$1.90E-1$	$2.47E-1$	$3.18E-1$

Next, we look for an approximation of the SIF applying the hybrid approach. The computational domain $\Omega_{Cp} = [0, 1] \times [0, 1]$ is split into the overlapping subdomains

$\widehat{\Omega}_1 = [0, 0.15] \times [0, 0.15]$ and $\Omega_2 = \Omega_{Cp} - ([0, 0.1] \times [0, 0.1])$. We compute the elasticity problem by the hybrid algorithm and determine the stress intensity factors K_I^{ha} with the J-integral method. These values are displayed in the last line of Table 6.

This example illustrates the computational capabilities and the accuracy of the hybrid approach.

6 Conclusion

An algorithm to compute the SIFs for a given crack in a highly heterogeneous plate is presented, which is both accurate and computationally cheap. In general, this algorithm may be applied successfully to materials which are homogenisable everywhere except in the vicinity of the crack tip. Also, it can be easily extended to plates with a small number of cracks. We note that the finite element based packages Abaqus and Comsol Multiphysics, in combination with Matlab, were used in the implementation of the algorithm and throughout the examples present in this work.

References

- A. Dimitrov, F.-G. B.; Schnack, E.** (2006): On three-dimensional effects in propagation of surface-breaking cracks. *CMES: Computer Modeling in Engineering & Sciences*, vol. 12, no. 1, pp. 1–25.
- Aliabadi, M. H.; López, M. H.** (1996): *Database of stress intensity factors*. Computational Mechanics Publications.
- Ashby, M. F.; Jones, D. R.** (1996): *Engineering materials 1, an introduction to their properties and applications*. Butterworth Heinemann.
- Aymerich, F.; Serra, M.** (2006): An ant colony optimization algorithm for stacking sequence design of composite laminates. *CMES: Computer Modeling in Engineering & Sciences*, vol. 13, no. 1, pp. 49–65.
- Broek, D.** (1986): *Elementary engineering fracture mechanics*. Kluwer Academic Publishers.
- Cherepanov, G. P.** (1979): *Mechanics of Brittle Fracture*. MacGraw-Hill.
- Cioranescu, D.; Donato, P.** (1999): *An introduction to homogenization*. Oxford University Press.

Fitzgerald, G.; Goldbeck-Wood, G.; Kung, P.; Petersen, M.; Subramanian, L.; J.Wescott (2004): Adaptive multiscale computational modelling of composite materials. *CMES: Computer Modeling in Engineering & Sciences*, vol. 5, no. 2, pp. 151–170.

Fitzgerald, G.; Goldbeck-Wood, G.; Kung, P.; Petersen, M.; Subramanian, L.; J.Wescott (2008): Materials modeling from quantum mechanics to the mesoscale. *CMES: Computer Modeling in Engineering & Sciences*, vol. 24, no. 3, pp. 169–183.

Freund, L. B. (1990): *Dynamic Fracture Mechanics*. Cambridge University Press.

Gato, C.; Shie, Y. (2008): Numerical simulations of dynamic fracture in thin shell structures. *CMES: Computer Modeling in Engineering & Sciences*, vol. 33, no. 3, pp. 269–292.

Guz, A. N.; J.Rushchitsky, J.; A.Guz, I. (2008): Comparative computer modeling of carbon-polymer composites with carbon or graphite microfibers or carbon nanotubes. *CMES: Computer Modeling in Engineering & Sciences*, vol. 26, no. 3, pp. 139–156.

H. Tada, P. C. P.; Irwin, G. R. (2000): *The Stress Analysis of Cracks Handbook*. ASME Press.

Hegen, D. (1997): *An Element-free Galerkin Method for Crack Propagation in Brittle Materials*. PhD thesis, Eindhoven University of Technology, 1997.

Hou, T.; Wu, X.; Cai, Z. (1999): Convergence of a multiscale finite element method for elliptic problems with rapidly oscillating coefficients. *Math. Comp*, vol. 227, no. 68, pp. 913–943.

Irwin, G. R. (1957): Analysis of stresses and strains near the end of a crack transversing a plate. *Trans. A.S.M.E., J. Applied Mechanics*, vol. 24, pp. 361–364.

Irwin, G. R. (1958): *Encyclopedia of Physics (Handbuch der Physik*, volume VI. Springer, Berlin.

Irwin, G. R. (1958): *Encyclopedia of Physics (Handbuch der Physik*, volume IV. Springer, Berlin.

Masuda, S.; Noguchi, H. (2006): Analysis of structure with material interface by meshfree method. *CMES: Computer Modeling in Engineering & Sciences*, vol. 3, no. 11, pp. 131–143.

Nobile, L.; Carloni, C. (2005): Fracture analysis for orthotropic cracked plates. *Compos. Struct.*, vol. 68, pp. 285–293.

Owen, D. R. J.; Fawkes, A. J. (1983): *Engineering Fracture Mechanics: Numerical Methods and Applications*. Pineridge Press.

Patrício, M.; Mattheij, R.; de With, G. (2008): Homogenisation with application to layered materials. *to be published in Math. Comput. Simul.*

Patrício, M.; Mattheij, R.; de With, G. (2008): Solutions for periodically distributed materials with localised imperfections. *CMES: Computer Modeling in Engineering & Sciences*, vol. 38, no. 2, pp. 89–118.

Pavliotis, G.; Stuart, A. M. (2007): Multiscale methods: averaging and homogenization. <http://www.maths.warwick.ac.uk/~stuart/book.pdf>, 2007.

Rice, J. R. (1968): A path independent integral and the approximate analysis of strain concentration by notches and cracks. *Transactions of ASME, Journal of Applied Mechanics*, vol. 35, pp. 79–386.

Sageresan, N.; Drathi, R. (2008): Crack propagation in concrete using meshless method. *CMES: Computer Modeling in Engineering & Sciences*, vol. 32, no. 2, pp. 103–112.

van Vroonhoven, J. C. W. (1996): *Dynamic Crack Propagation in Brittle Materials: Analyses Based on Fracture and Damage Mechanics*. PhD thesis, Eindhoven University of Technology, 1996.

Wang, H.; Wang, S. (2008): Analysis of dynamic fracture with cohesive crack segment method. *CMES: Computer Modeling in Engineering & Sciences*, vol. 35, no. 3, pp. 253–274.

Westergaard, H. M. (1939): Bearing pressures and cracks. *Trans. A.S.M.E., J. Applied Mechanics*.

Zehnder, A. (2007): *Lecture Notes on Fracture Mechanics*. Cornell University.

